Progress In Electromagnetics Research C, Vol. 110, 91–102, 2021

Design of Dual-Band Conformal AMC Integrated Antenna for SAR Reduction in WBAN

Bidisha Hazarika, Banani Basu*, and Arnab Nandi

Abstract—A wearable, miniaturized, dual-band, Artificial Magnetic Conductor (AMC) integrated antenna operating on ISM band (2.38–2.47 GHz) and WLAN band (5.11–5.31 GHz) is proposed for Wireless Body Area Network (WBAN). A dumbbell shaped unit-cell is designed to achieve zero reflection phase and modified material characteristics. When 2×2 array of dumbbell shaped AMC is put underneath the monopole, the antenna gain increases up to 9.5 dB and 8.1 dB at 2.43 GHz and 5.2 GHz, respectively. Different bending conditions have been considered to confirm the robustness of the AMC antenna. Debye model is used to approximate the dielectric properties within phantom tissue model. Antenna shields most of the backward radiation and reduces the specific absorption rate (SAR) of the integrated antenna by more than 95% in 1-g of phantom hand tissues at both the frequencies. The acquired results exhibit that the AMC antenna is more secure for on body applications.

1. INTRODUCTION

With the recent growth of WBAN system, it is crucial to design an antenna to be implanted inside and outside the human body. Antennas used for wearable applications are essentially compact, light weight, and mechanically robust. Use of AMC to achieve low profile, high gain, and unidirectional antenna is studied in many articles [1–4]. Application of AMC to achieve improved radiation performance and higher isolation in dual bands is reported in [1]. [2] presents an AMC loaded antenna resonating at 2.45/5.8 GHz to reduce the SAR. Article [3] has proposed a metamaterial based high gain antenna for radar and BAN applications. A low-profile left-handed metamaterial based multiband antenna for wireless application is proposed in [4]. Another high gain metamaterial antenna for long range radio frequency identification (RFID) applications has been reported in [5]. In [6], an AMC planar antenna is introduced with 43.3% SAR reduction. A low-profile antenna based on AMC is designed to lower SAR value for WLAN application [7]. In [8], a wearable monopole in both flat and bent conditions has been designed. A dual-band AMC antenna is presented to lessen SAR up to 70% [9]. A wearable antenna with reduced SAR has been reported for indoor-outdoor positioning system [10]. [11] has introduced a low SAR, dual-band wearable antenna to perform different structural deformation when it is placed near artificial human body. Reduction of the SAR on different human body parts has become a topic of recent interest for implantable and wearable antennas.

The article presents a novel low-profile, conformal, dual-band AMC integrated antenna at 2.43 GHz and 5.2 GHz. The AMC layer consists of a dumbbell-shaped unit-cell structure which possesses an effective zero reflection phase at 2.5 GHz and bandwidth from 2.45 to 2.55 GHz limited within $\pm 90^\circ$ reflection phase. The reported AMC layer attains double-negative permittivity and permeability, and negative refractive index in the designated bands. A monopole with rectangular slot covering 2.5 GHz band is designed to integrate with AMC. The AMC integrated slotted monopole having 5 mm separation

Received 12 December 2020, Accepted 9 February 2021, Scheduled 21 February 2021
* Corresponding author: Banani Basu (banani.basu@gmail.com).
The authors are with the Department of Electronics and Communication Engineering, National Institute of Technology Silchar, Silchar, Cachar, Assam 788010, India.

proffers dual operating bands and 9.5 dB and 8.1 dB gains at the respective bands. The integrated antenna increases the front to back radiation to 6.3 dB and 21.2 dB at the two frequencies and has E-field *co-x* pol intensity differences of 10.23 dB and 11.15 dB, and H-field intensity differences of 13.62 dB and 12.21 dB at 2.43 GHz and 5.2 GHz, respectively. Excellent radiation efficiency values of 95% and 98.5% are achieved at both the bands. The AMC integrated antenna is deformed over different bending radii to see the robustness of the antenna. Dielectric properties of the antenna are characterized at both the bands when it is placed near human body. The AMC integrated antenna is placed on male and female hand phantom models for 1-g tissues to see the maximum SAR performance. The values agree well with that of the FCC and ICNIRP standards.

2. ANTENNA AND AMC DESIGN

Simulation is carried out to design AMC layer and a slotted monopole antenna for WBAN applications. A dumbbell shaped AMC unit-cell is developed to be operated at 2.5 GHz. Different material characteristics of the AMC layer have been studied to examine the double negative properties ($\varepsilon < 0$, $\mu < 0$).

2.1. Configuration of AMC

The proposed dumbbell shaped unit-cell is exhibited in Fig. 1(a). A Roger RO3003 flexible substrate with $\varepsilon_r = 3$, $\tan\delta = 0.0013$, and thickness = 1.5 mm is used in the design. The AMC surface is implemented by zero reflection phase characterization. It is seen from Fig. 1(b) that the exact point of the zero phase reflection is positioned at 2.5 GHz with a small bandwidth from 2.45 GHz to 2.55 GHz within $\pm 90^\circ$ phase values [12] where signal interference is obtained between the incident wave and reflected wave. Master and slave boundaries and Floquet ports are used to establish the simulation for infinite periodic array in HFSS.

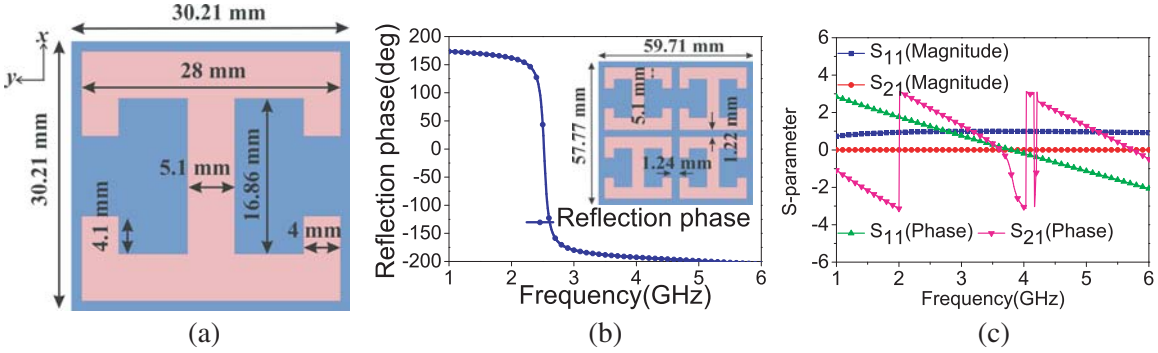

Figure 1. (a) Design of unit-cell. (b) Design of 2×2 AMC and zero reflection phase of unit-cell. (c) S-parameters of unit-cell.

2.2. Material Characteristics of Unit-Cell

The response of a design is determined through its permittivity (ε) and permeability (μ). Scattering parameter-retrieval [12] is an effective method to extricate these material properties. The characterization of the AMC requires a limitless number of unit-cells towards the lattice vectors direction. These properties are attained by giving periodic boundaries to the unit-cell and the S-parameters: S_{11} and S_{21} are extricated and presented in Fig. 1(c). ε and μ are extricated by utilizing S_{11} and S_{21}, and shown in Figs. 2(a) and (b) correspondingly. In the figure it is proved that the designed AMC offers small and negative ε and μ at the respective bands. It provides positive wave impedance (z) and small negative index of refraction (n) which are eventually reflected in Figs. 2(c) and (d).

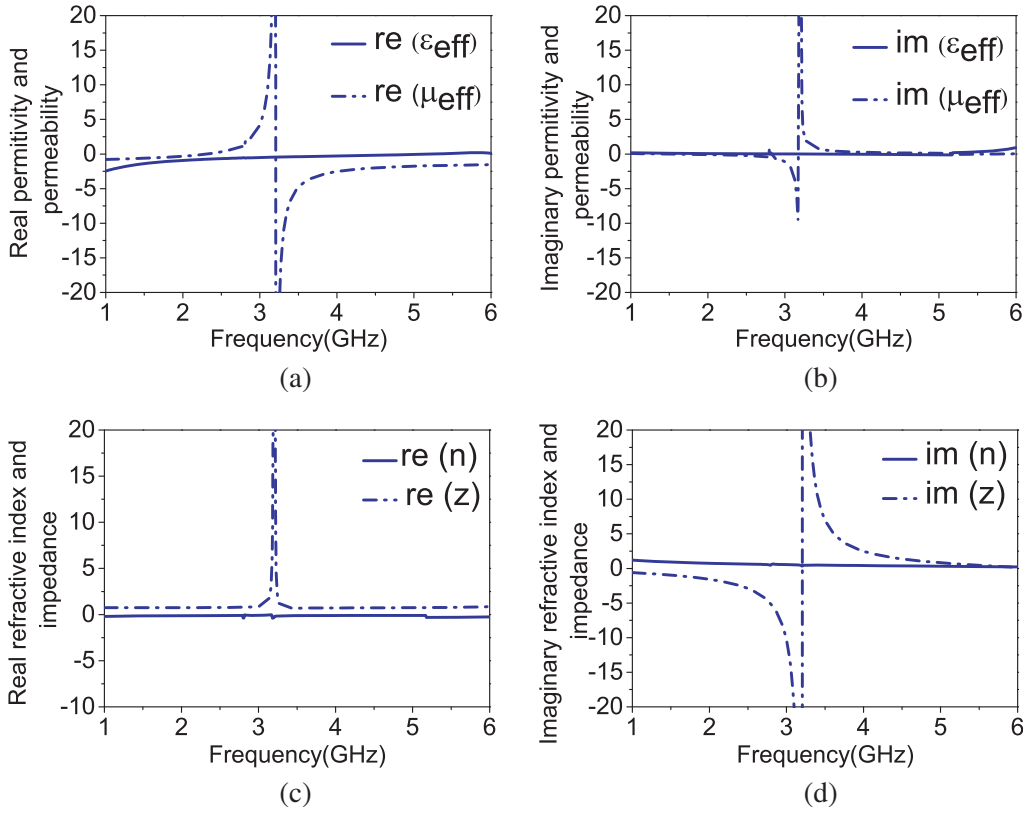

Figure 2. Material features of unit-cell. (a) Real μ, ε. (b) Imaginary μ, ε. (c) Real n, z and (d) Imaginary n, z.

2.3. Antenna Configuration

The monopole antenna and its S_{11} are shown in Figs. 3(a) and (b). The monopole is realized on the same Rogers RO3003 substrate as used for AMC. Essential design parameters are precisely adjusted so that it matches well with the AMC. The antenna operates at 2.5 GHz, and the optimized parameters of the radiator are recorded in Table 1.

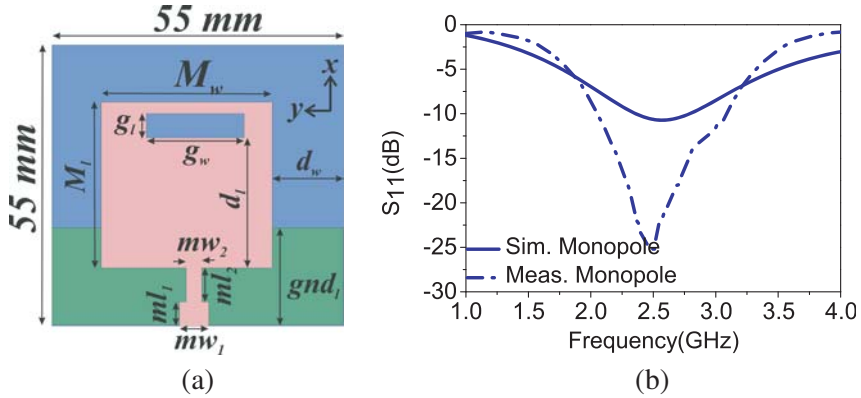

Figure 3. (a) Configuration and (b) S_{11} of monopole antenna.

Table 1. Optimized monopole parameters (Unit: mm).

Design Parameters	M_w	M_l	mw_1	mw_2	ml_1	ml_2
Values	34	34	6	3.2	5	7
Design Parameters	g_l	g_w	d_w	d_l	gnd_l	
Values	5	20	11.5	40	20	

2.4. Integration of Proposed AMC Antenna

The AMC integrated antenna and its prototype are presented in Figs. 4(a) and (b). The h_air value is moderately adjusted to produce better impedance matching and realized using foam spacers of height 5 mm and dielectric constant near 1 between the antenna and AMC layer at the four corners. The monopole antenna is positioned on top of the AMC surface to attain in-phase reflection characteristics at both the frequency bands. The reflection characteristic of the AMC layer mentioned in Fig. 5 suggests that the monopole can be positioned at 5 mm height above the AMC layer without affecting its radiation efficiency [Fig. 8(b)] at the designated frequency. Considering the dimension of the feed line and radiation analysis of the antenna, we have selected the AMC layer with a 2×2 unit-cell array having the dimension of $57.77 \times 59.71\ \text{mm}^2$. Fig. 1(b) shows the physical design of the dumbbell-shaped 2×2 AMC unit-cells array.

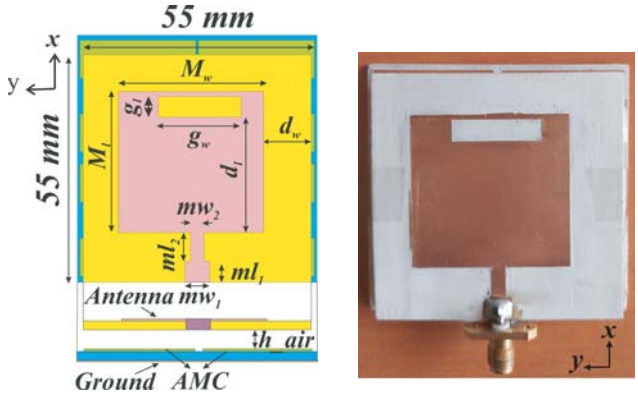

(a) (b)

Figure 4. (a) Configuration of integrated antenna. (b) Prototype of fabricated antenna.

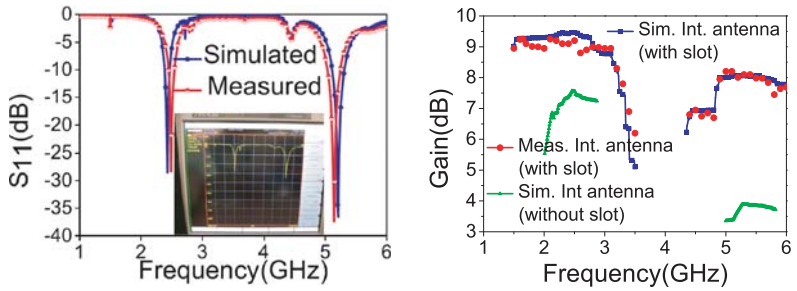

(a) (b)

Figure 5. (a) S_{11} and, (b) gain of integrated antenna.

3. RESULTS AND DISCUSSION

The integration of monopole with the AMC is accomplished to improve the radiation performances. According to Fig. 1(b), the AMC structure offers zero phase reflection at 2.5 GHz. The proposed antenna also shows weak resonance at 2.5 GHz. AMC antenna provides excellent impedance matching at 2.5 GHz. Again at 5.2 GHz, the space phase caused due to the gap between radiator and the AMC modifies the effective reflection phase and establishes the impedance matching condition. The integrated antenna also gives good front-to-back radiation ratio and co- and x-pol intensity difference up to 14 dB for both the bands.

3.1. S_{11} Parameter

The S-parameters of the integrated antenna, measured by the Anritsu vector network analyzer MS2037C, is exhibited in Fig. 5(a). Fig. 5(a) depicts that the simulated reflection coefficient bandwidth equivalent to $S_{11} < -10$ dB is spaced at 2.38–2.47 GHz and 5.11–5.31 GHz. The monopole resonating near 2.5 GHz ha used rectangular slot to make antenna layer inductive at 5.2 GHz which upon integration with the capacitive AMC layer excites two resonating bands at 2.43 GHz and 5.2 GHz.

3.2. Gain, Radiation Pattern and FB Ratio

When the AMC layer with full ground at the back is located near the monopole, it functions as an infinite layer, reduces the edge effect, and improves the spill over efficiency. The gain, radiation pattern, and FBR of the integrated antenna are measured in an anechoic chamber with pyramidal shaped absorbers using Anritsu MS2037 VNA. The slotted monopole placed at a distance 5 mm above the AMC surface proffers gain nearly equal to 9.5 dB and 8.1 dB at both the bands as in Fig. 5(b) [13, 14]. Measured gain of the AMC antenna shows maximum discrepancy of 0.6 dB compared to the simulated gain because of fabrication error. The 2×2 array AMC effectively has transformed the spherical-like phase contour of the radiated wave into in-phase planar pattern and enhanced the antenna gain. Without the slot the AMC antenna offers 7.5 dB and 3.7 dB gains at the two bands.

Figures 6(a)–(d) show the simulated and measured E- and H-field radiation features (far-field) of the AMC integrated antenna at the two frequencies. At 2.43 GHz, the radiation intensity differences

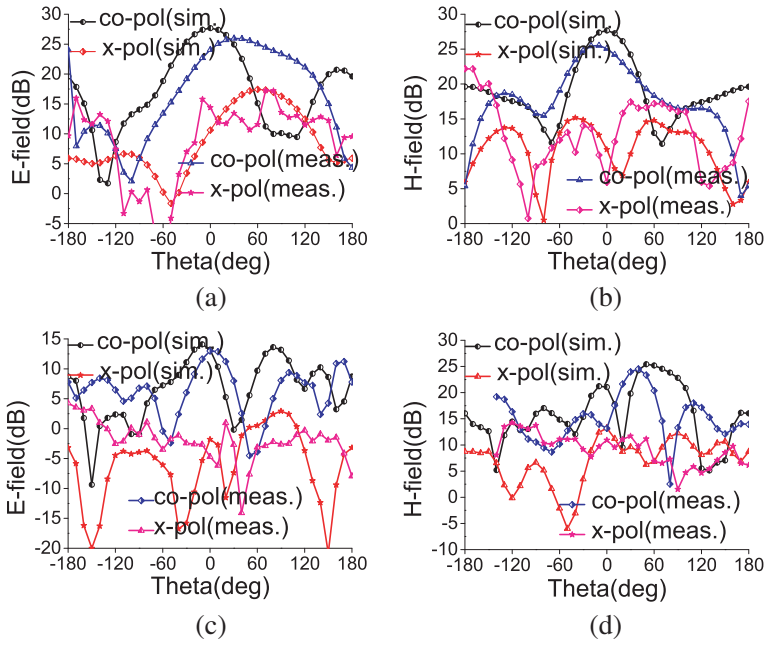

Figure 6. Simulated and measured far-field distributions of AMC integrated antenna. (a) E-field and (b) H-field at 2.43 GHz. (c) E-field and (d) H-field at 5.2 GHz.

between E- and H-field *co-x* pol at broadside direction are 10.23 dB and 13.62 dB respectively. On the other hand, the measured AMC antenna has E- and H-field radiation intensity differences between *co-pol* and *x-pol* equal to 8.7 dB and 8.08 dB. At 5.2 GHz, the E- and H-field radiation intensity differences at broadside direction are 11.15 dB and 12.21 dB, respectively. However, the measured E-field and H-field radiation intensity differences at 5.2 GHz are 11.91 dB and 12.82 dB respectively [15]. The simulated and measured radiation patterns are varied due to fabrication and cabling error, and air bubble is present in the foam spacer.

Figure 7 shows that the phase of the E-field is relatively stable within main lobe directions at 2.43 GHz and 5.2 GHz when the antenna is incorporated with the AMC. Thus the AMC layer nullifies the out-of-phase radiation and improves radiation gain.

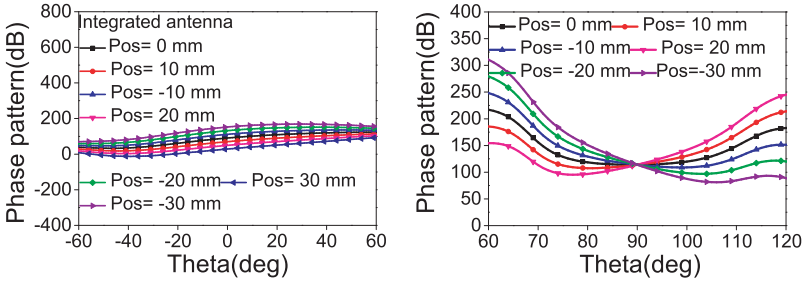

Figure 7. Phase center of integrated antenna at (a) 2.43 GHz and (b) 5.2 GHz.

The integrated antenna gives FBR values of 6.3 dB at 2.43 GHz and 21.2 dB at 5.2 GHz [Fig. 8(a)] [13]. The radiation efficiency values of the integrated antenna are 0.95 at 2.43 GHz and 0.985 at 5.2 GHz because of integration of AMC below the monopole, as displayed in Fig. 8(b).

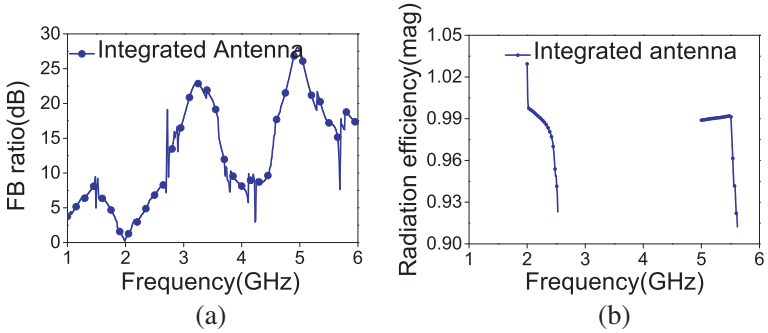

Figure 8. Integrated antenna parameters. (a) FB ratio. (b) Radiation efficiency.

Figures 9(a) and (b) present the current distributions on the antenna without slot at 2.43 GHz and 5.2 GHz. Figs. 9(c) and (d) show the current distributions on the antenna slot at 2.43 GHz and 5.2 GHz. Due to the slot on the monopole, the current path redistributes, and surface current distribution depresses signifying that the antenna with slot radiates more electromagnetic energy.

4. CONFORMAL ANTENNA ANALYSIS

For WBAN application in real scenario, the antenna undergoes physical deformation, which is approximated with different bending angles. Bending radii of R_a = 150 mm, 90 mm, 40 mm, 35 mm, 30 mm, 25 mm, 20 mm, and 15 mm are assigned to the AMC antenna, and the results obtained are analyzed and presented in Fig. 10. We have also designed a reference patch antenna at 2.4 GHz for evaluating the three bending responses. As we vary the bending radius from 150 mm to 15 mm for

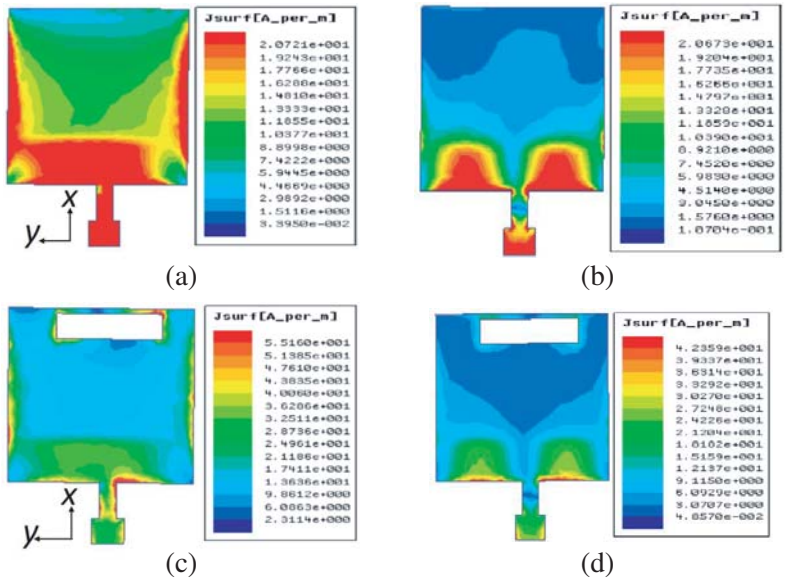

Figure 9. Simulated surface current distribution at (a) 2.43 GHz without slot, (b) 5.2 GHz without slot, (c) 2.43 GHz with slot, (d) 5.2 GHz with slot.

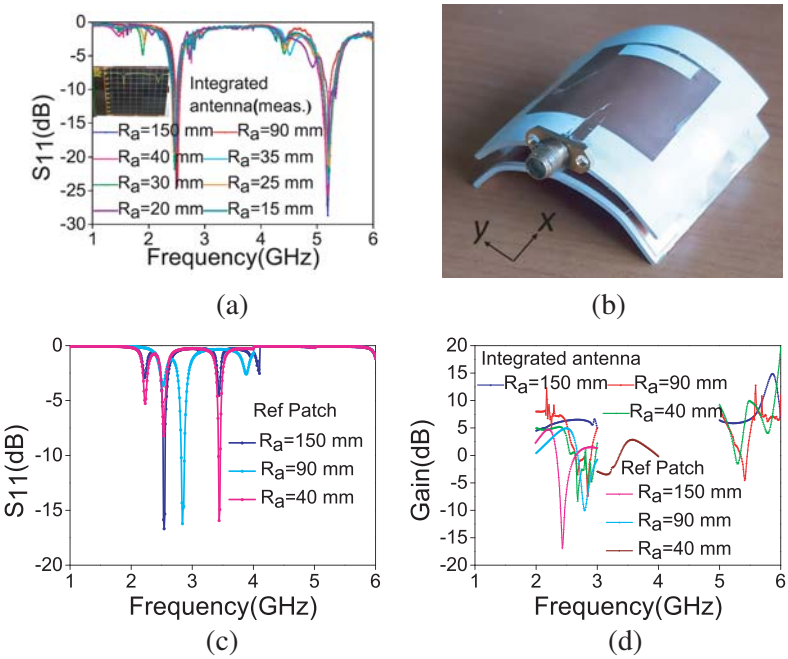

Figure 10. (a) S_{11} of conformal integrated antenna. (b) Conformal prototype. (c) S_{11} of conformal ref patch and (d) gain of integrated and ref patch for different R_a.

the AMC antenna, the 2.43 GHz frequency band shifts with the maximum deviation up to 0.09 GHz, and the 5.2 GHz frequency band swings with the maximum deviation up to 0.24 GHz as represented in Fig. 10(a). It is also observed from Fig. 10(a) that the S_{11} curve deteriorates as the bending radius increases. The related conformal structure is shown in Fig. 10(b). For reference patch antenna, due to bending, the peak resonant frequency shifts significantly to 2.64 GHz, 2.84 GHz, and 3.44 GHz from 2.4 GHz as in Fig. 10(c). It is seen from Fig. 10(d) that the broadside simulated gain profile of the

integrated antenna at $R_a = 150$ mm offers a peak gain of 8.4 dB and 7.5 dB at the dual frequency bands. However, according to Fig. 10(d), the reference patch antenna suffers from substantial gain drop in the respective bands owing to the shifting of resonating frequency due to bending and the broadening of the radiation beamwidth. From this analysis, we can infer that the performances of both the structures, original and conformal AMC based antennas, are in accordance well. It happens that as the antenna is deformed around any surface, the effective length of the antenna increases. The integrated antenna consists of two parts: the monopole antenna and AMC surface. When length increases, the monopole becomes inductive, and AMC becomes capacitive. At resonances, the inductive and capacitive effects nullify each other, and the antenna proffers robustness in bending.

5. IMPACT ON HUMAN BODY

The simulated and measured S_{11} of the antenna while being placed on the phantom model and on body are exhibited in Fig. 11(a). While the integrated antenna is put on male phantom hand, the frequency is shifted to 2.41 GHz and 5.12 GHz, respectively [Fig. 11(a)]. In the case of female phantom hand, the frequency shifts to 2.42 GHz and 5.17 GHz [Fig. 11(a)], respectively. The conformal antenna, with a bending radius of 150 mm, operates at 2.44 GHz and 5.28 GHz in free space. As the test antenna is positioned on male and female phantom hands, the lower frequency band is shifted to 2.55 GHz and 2.48 GHz on male and female hands, respectively, as shown in Fig. 11(b). Again in the case of higher operating frequency band, the operating frequency shifts to 5.18 GHz and 5.15 GHz as loaded on male and female hands individually. This shifting occurs because of the dielectric variation of the antenna in the presence of human tissues. A reference patch antenna operating at 2.4 GHz is also placed on both male and female phantom hands. While the antenna is situated at 10 mm apart from the human hand phantom, the operating frequency shifts to 3.25 GHz and 3.26 GHz for male and female hands, respectively [Fig. 11(c)].

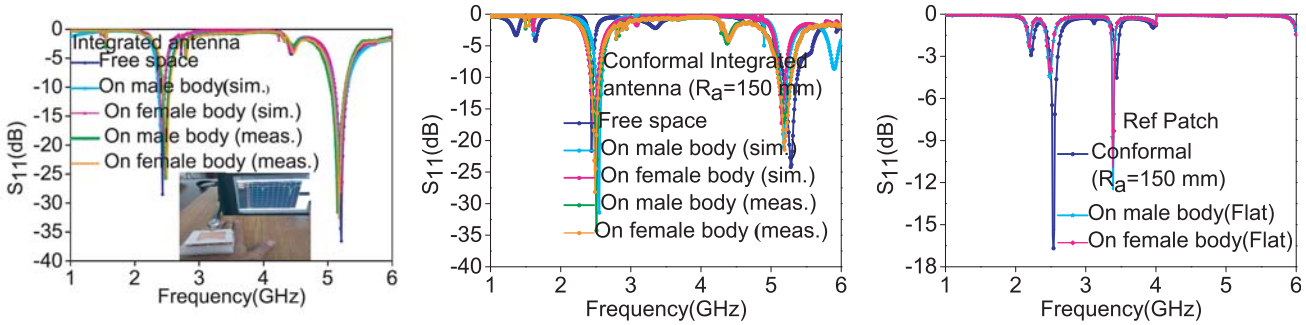

Figure 11. Simulated and measured S_{11} of integrated antenna on (a) flat and (b) bent condition, (c) simulated S_{11} of patch antenna on bent and flat condition.

6. SAR EVALUATION FOR ARTIFICIAL HUMAN MODEL ANALYSIS

The Specific Absorption Rate (SAR) is the rate of EM power absorbed per unit mass of body tissues. According to the IEEE C95.1-1999, SAR values should not be greater than 1.6 W/kg over 1-g of tissues. Before utilizing the antenna for WBAN application, the SAR is calculated considering the input power equal to 100 mW.

The amount of RF exposure on human body is related to the conductivity of the human tissues (σ), mass density (ρ), and the intensity of the electric-field (E). As the absorbed power is associated with the E-field to the highest extent, the maximum SAR value needs to be listed in the regions where E-field strengths are maximum. An artificial multi-layered human tissue model as shown in Fig. 12 has been used to perform the on body SAR analysis. This artificial model consists of skin, fat, muscle, and bone with individual permittivity, conductivity, thickness, and mass-density values. To record SAR,

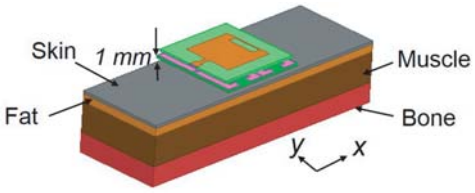

Figure 12. Flat multi-layered human tissue model.

AMC-based antenna is located at 1 mm apart from the air-skin interface. The relative permittivity and conductivity of different tissues at different frequencies due to the placement of the proposed antenna are simulated using Debye model [16] and plotted in Fig. 13. Finally, the multi-layered tissue properties including SAR values at two designated frequencies are listed in Table 2.

Table 2. Permittivity, conductivity and SAR values using Debye model.

Human tissue layers	Debye model						
		ε		σ		SAR (W/kg)	
	ε_∞	2.43 GHz	5.2 GHz	2.43 GHz	5.2 GHz	2.43 GHz	5.2 GHz
Skin	4	4.00002	4.00001	0.00267	0.00267	0.225	0.146
Fat	2.5	2.50003	2.50002	0.00167	0.00167	0.21	0.14
Muscle	4	4.00001	4.000002	0.00267	0.00267	0.247	0.124
Bone	2.5	2.50002	2.500008	0.00167	0.00167	0.131	0.00453

7. SAR EVALUATION FOR HUMAN PHANTOM MODEL

As presented in Fig. 14, the human phantom model for hand developed by ANSYS HFSS is exploited for testing. The separation (d) between the skin and AMC antenna is set at 10 mm. Table 3 presents the SAR value of the flat and bent monopole and integrated antennas for 1-g of tissues at the respective bands. It is seen that maximum SAR of the flat and bent antennas on male and female hands at 1-g of tissues are below the existing regulations [13, 14] in all the cases. However, the SAR values of the conformal antenna in every cases are slightly higher than that of the flat one. In comparison to the monopole antenna alone: the SAR reduction acquired from the AMC antenna is 99.9% at 2.43 GHz

Table 3. Simulated SAR values of flat and bent ($R_a = 150$ mm) monopole and AMC integrated antenna on human phantom hand (Unit: W/kg).

Parameters	Flat (F) and Bent (B) ($R_a = 150$ mm) Monopole		Flat (F) AMC antenna		Bent (B) ($R_a = 150$ mm) AMC antenna	
Frequency (GHz)	1-g (male)	1-g (female)	1-g (male)	1-g (female)	1-g (male)	1-g (female)
2.5 (Mono)/ 2.43 (Int) GHz	0.404 (F)	0.682 (F)	0.00037	0.000833	0.0019	0.0091
	0.413 (B)	0.870 (B)				
5.2 GHz			0.000686	0.000893	0.00245	0.0288

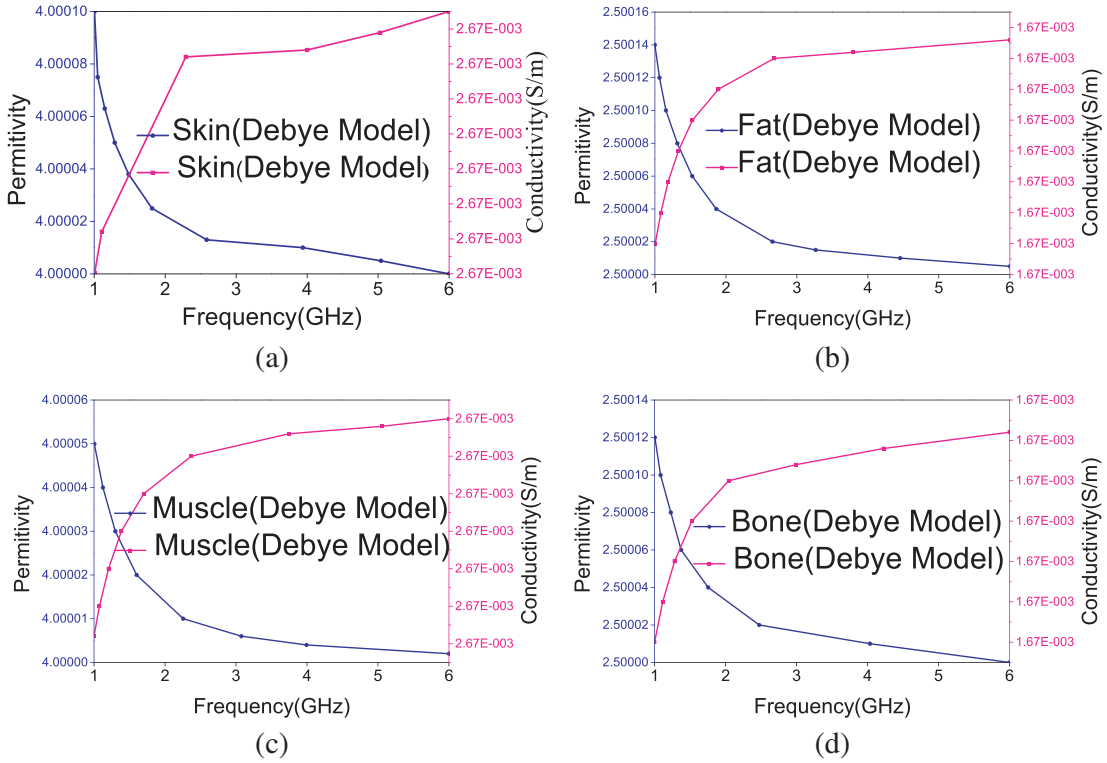

Figure 13. Permittivity and conductivity of tissues. (a) Skin, (b) fat, (c) muscle and (d) bone for Debye model.

when it is on male hand. In the same environment, at 5.2 GHz, the reduction for 1-g body tissues is 99.83%. In comparison to the deformed monopole antenna, the bent AMC antenna offers 99.5% reduction at 2.43 GHz on male phantom. However, at 5.2 GHz, the curved AMC antenna achieved 99.4% reduction in SAR value with respect to the SAR of the monopole at 2.5 GHz, when it is on male phantom hand. Table 4 compares the features of the proposed antenna in terms of S_{11}, gain, efficiency, ka, and SAR values with those of the existing implantable antennas described in literature [6–9] and substantiates the superiority of the proposed one. Here k = free-space wave number and a = radius of the sphere confining the radiator [17]. In the proposed design, antenna has the ka value equal to 1.22 and considered as a compact antenna. So the antenna offers high Q value which gives high gain and leads to lower BW of 3.7% and 3.8% at 2.43 GHz and 5.2 GHz.

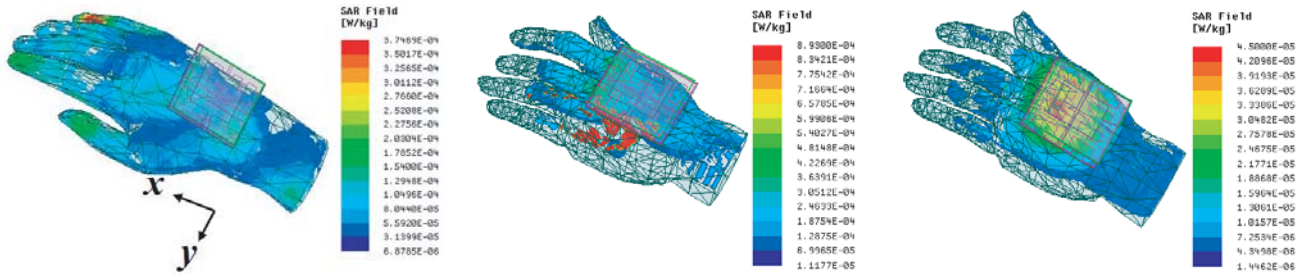

Figure 14. Simulated SAR of flat and bent AMC antenna at 2.43 GHz. (a) 1-g of tissues on male hand. (b) 1-g of tissues on female hand. (c) 1-g on female hand at 5.2 GHz.

Table 4. Comparison of antenna characteristics described for WBAN applications.

Ref. No.	Size	Bands	Gain	Efficiency	ka	SAR
[6]	$0.190\lambda \times 0.123\lambda$	1.96 GHz, 1.97 GHz, 1.98 GHz	4.668 dB, 4.693 dB, 4.722 dB	n/a	0.37	0.17 W/kg, 0.178 W/kg, 0.163 W/kg (10-g on hand)
[7]	$1.12\lambda \times 1.12\lambda$	5.2 GHz, 5.8 GHz	6.1 dBi, 5.9 dBi	92%, 91%	3.93	0.22 W/kg, 0.18 W/kg (1-g on head)
[8]	$0.316\lambda \times 0.274\lambda$	2.45 GHz	8.41 dBi	71%	1.15	0.33 W/kg (1-g on artificial layer)
[9]	$0.246\lambda \times 0.2\lambda$	2.45 GHz, 5.8 GHz	5.2 dB, 7.7 dB	61.3%, 67.2%	0.51	2.48 W/kg, 3.33 W/kg (1-g on forearm)
[13]	$0.367\lambda \times 0.486\lambda$	3.5 GHz, 5.8 GHz	9.373 dB, 6.634 dB	83.5%, 96.5%	1.89	0.0683 W/kg, 0.333 W/kg (1-g on hand)
[14]	$0.225\lambda \times 0.146\lambda$	2.45 GHz	6.51 dBi	74.8%	0.833	0.22 W/kg (1-g on hand)
[Proposed work]	$0.492\lambda \times 0.478\lambda$	2.43 GHz, 5.2 GHz	9.5 dB, 8.1 dB	95%, 98.5%	1.22	0.00037 W/kg, 0.000686 W/kg (1-g on hand)

8. CONCLUSION

This paper has proposed a dual-band, wearable AMC integrated antenna for WBAN applications. It utilizes a 2×2 array of dumbbell-shaped metallic sheet backed AMC for attaining higher gain and lower SAR on human phantom hand. The realized antenna accomplishes higher gains of 9.5 dB and 8.1 dB and efficiencies of 95% and 98.3% at the two frequency bands. *Co-pol* and *x-pol* radiation intensity differences of 10.23 dB and 11.15 dB for E-field and 13.62 dB and 12.21 dB for H-field have been achieved at 2.43 GHz and 5.2 GHz, respectively. The multi-layered AMC has further reduced the backward electromagnetic radiation and increases the FB radiation ratio up to 6.3 dB and 21.2 dB at lower and upper frequency bands, respectively. Different conformal performances have demonstrated the robustness of the antenna. The impact of the human body loading of the integrated antenna is investigated using Debye model. While the monopole is integrated with AMC, the SAR performance decreases more than 95% on both flat and bent conditions, which is enough within the limits specified by ICNIRP.

REFERENCES

1. Zhai, H., K. Zhang, S. Yang, and D. Feng, "A low-profile dual-band dual-polarized antenna with an AMC surface for WLAN applications," *IEEE Antennas and Wireless Propagation Letters*, Vol. 16, 2692–2695, 2017.
2. Mersani, A., L. Osman, and J.-M. Ribero, "Performance of dual-band AMC antenna for wireless local area network applications," *IET Microwave and Antenna Propagation*, Vol. 12, No. 6, 872–878, 2018.

3. Misra, P., S. S. Pattnaik, W. Cao, S. Shi, Q. Wang, and W. Zhong, "Metamaterial loaded fractal based interdigital capacitor antenna for communication systems," *Progress In Electromagnetics Research M*, Vol. 16, 2473–2476, 2018.
4. Ayd, A. and R. Rad, "Low-profile MIMO antenna arrays with left-handed metamaterial structures for multiband operation," *Progress In Electromagnetics Research M*, Vol. 89, 1–11, 2020.
5. Moreira, E. C., R. O. Martins, B. M. S. Ribeiro, and A. S. B. Sombra, "A novel gain-enhanced antenna with metamaterial planar lens for long-range UHF RFID applications," *Progress In Electromagnetics Research B*, Vol. 85, 143–161, 2019.
6. Kwak, S. I., D.-U. Sim, J. H. Kwon, and Y. J. Yoon, "Design of PIFA with metamaterials for body-SAR reduction in wearable applications," *IEEE Transactions on Electromagnetic Compatibility*, Vol. 59, No. 1, 297–300, 2017.
7. Cao, Y. F., X. Y. Zhang, and T. Mo, "Low-profile conical-pattern slot antenna with wideband performance using artificial magnetic conductors," *IEEE Transactions on Antennas and Propagation*, Vol. 66, No. 5, 2210–2218, 2018.
8. Alemaryeen, A. and S. Noghanian, "Crumpling effects and specific absorption rates of flexible AMC integrated antennas," *IET Microwave and Antenna Propagation*, Vol. 12, No. 4, 627–635, 2018.
9. Wang, M., Z. Yang, J. Wu, J. Bao, J. Liu, L. Cai, T. Dang, H. Zheng, and E. Li, "Investigation of SAR reduction using flexible antenna with metamaterial structure in wireless body area network," *IEEE Transactions on Antennas and Propagation*, Vol. 66, No. 6, 3076–3086, 2018.
10. Lee, H., J. Tak, and J. Choi, "Wearable antenna integrated into military berets for indoor/outdoor positioning system," *IEEE Antennas and Wireless Propagation Letters*, Vol. 16, 1919–1922, 2017.
11. Hazarika, B., B. Basu, and A. Nandi, "Design of antennas using artificial magnetic conductor layer to improve gain, flexibility, and specific absorption rate," *Microwave and Optical Technology Letters*, Vol. 62, No. 12, 3928–3935, 2020.
12. Hazarika, B., B. Basu, and A. Nandi, "An artificial magnetic conductor-backed monopole antenna to obtain high gain, conformability, and lower specific absorption rate for WBAN applications," *International Journal of RF and Microwave Computer-aided Engineering*, Vol. 30, No. 12, 1–9, 2020.
13. Atrash, M. E., M. A. Abdalla, and H. M. Elhennawy, "A wearable dual-band low profile high gain low SAR antenna AMC-backed for WBAN applications," *IEEE Transactions on Antennas and Propagation*, Vol. 67, No. 10, 1–10, 2019.
14. Atrash, M. E., M. A. Abdalla, and H. M. Elhennawy, "A compact highly efficient-section CRLH antenna loaded with textile AMC for wireless body area network applications," *IEEE Transactions on Antennas and Propagation*, doi: 10.1109/TAP.2020.3010622.
15. Ghosh, A., S. Chakraborty, S. Chattopadhyay, A. Nandi, and B. Basu, "Rectangular microstrip antenna with dumbbell shaped defected ground structure for improved cross polarised radiation in wide elevation angle and its theoretical analysis," *IET Microwave and Antenna Propagation*, Vol. 10, No. 1, 1–11, 2016.
16. Gabriely, S., R. W. Lau, and C. Gabriel, "The dielectric properties of biological tissues: III. Parametric models for the dielectric spectrum of tissues," *Physics Medical Biology*, Vol. 41, No. 11, 2271–2293, 1996.
17. Sievenpiper, D. F., D. C. Dawson, M. M. Jacob, T. Kanar, S. Kim, J. Long, and R. G. Quarfoth, "Experimental validation of performance limits and design guidelines for small antennas," *IEEE Transactions on Antennas and Propagation*, Vol. 60, No. 1, 8–19, 2012.